ChemComm

Accepted Manuscript

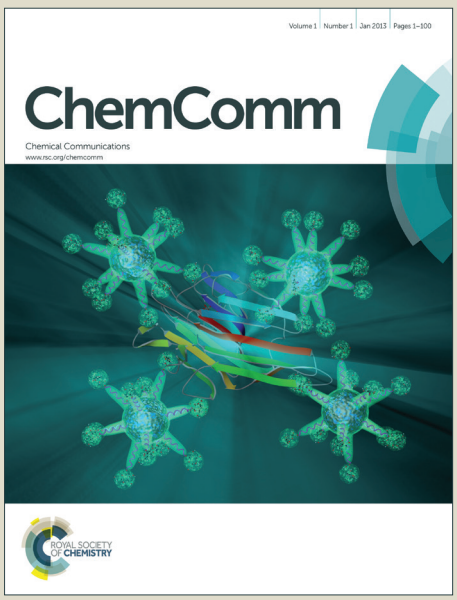

ROYAL SOCIETY OF CHEMISTRY

www.rsc.org/chemcomm

Journal Name

RSCPublishing

COMMUNICATION

A new approach to nanoscopic rare earth metal fluorides: the fluorolytic sol-gel synthesis of ytterbium fluoride

Cite this: DOI: 10.1039/x0xx00000x

Received ooth January 2012,
Accepted ooth January 2012

DOI: 10.1039/x0xx00000x

www.rsc.org/

L. Schmidt, A. Dimitrov and E. Kemnitz*[a]

A new approach for the preparation of *approx.* 5 nm sized ytterbium fluoride nanoparticles based on the fluorolytic sol-gel route is reported. DLS, TEM, IR and XRD were used to characterize the particles as well as the aging behavior of the sols. Furthermore, a new Yb^{III} complex was isolated from the precursor solution and characterized by X-ray single crystal structure determination.

New approaches to the treatment of dental caries have prompted the search for new restorative materials that can not only restore the decayed tooth but also inhibit the demineralization of tooth enamel (bacterial growth) and therefore prevent the recurrence of caries.[1] For several years now fluoride is well known for its effectiveness in caries prevention. A variety of cariostatic mechanisms of fluoride action are involved in order to reduce dental caries formation.[2]
Metal fluorides hold great promise in dentistry as inorganic fillers in dental composites providing mechanical strength and chemical stability, a decrease in solubility and therefore a long-term fluoride release.[3,4] Additionally oxides, fluorides and carbonates of lanthanum, hafnium, strontium and ytterbium are added for radiopacity in order to guarantee a precise radiographic diagnosis of carious lesions adjacent to the filling material. For some years now, rare earth (RE) metal fluorides are used as inorganic filling material in dentistry due to their ability to increase the efficiency of X-ray contrast and at the same time to provide a long-term fluoride release.[5] There has been a growing interest in using nanoparticles in order to improve the above mentioned properties. In general, nano-structured inorganic particles are claimed to act as antibacterial agents and improve the strength and mechanical properties of dental restorative materials.[6,7] Usually, RE metal fluorides are incorporated as a powder into the dental material. The average primary particle sizes which are reported vary thereby being in the range of 30-700 nm. Many chemical synthesis techniques have been developed to prepare nanoscopic RE metal fluorides. Usually, nanoscopic RE fluorides are prepared by autoclaving RE precursors in the presence of fluorinating agents at higher temperatures (hydrothermal method)[8], thermal decomposition of RE precursors (usually trifluoroacetates)[9,10] or using ionic liquids[11]. In recent years, the polyol-mediated synthesis [12] and the OA/ionic liquid two-phase method[13,14] have been developed to enable controllable synthesis of RE metal fluorides. Each of these methods has its own advantages and disadvantages depending on the requirements for nanomaterials. However, all these reported methods allow obtaining RE nanocrystalline fluorides as powder samples.
The fluorolytic sol-gel[15,16] synthesis represents an easy and mild chemical route for the preparation of nanoscopic metal fluorides which are examined for their properties and applicability. In this paper we report for the first time the preparation of ytterbium(III) fluoride sols with homodispersed particles of *approx.* 5 nm *via* the fluorolytic sol-gel synthesis, the advantage of this method being an easy access to even large amounts of these materials. Dynamic light scattering (DLS), high resolution transmission electron microscopy (HRTEM), infrared spectroscopy (IR) and X-ray powder diffraction (XRD) are used to characterize the final products.

The formation of ytterbium fluoride sols proceeds *via* the fluorolytic sol-gel synthesis. (Full experimental procedure is available in the ESI†) The anhydrous ytterbium acetate was converted into a ytterbium(III)-acetate-trifluoroacetate to give a transparent precursor solution. It has to be noted, that by using both the ytterbium acetate and ytterbium trifluoroacetate as precursors sedimentation of agglomerated particles is observed. Only by a modification of anhydrous ytterbium acetate with trifluoroacetic acid we obtained a suitable precursor for the preparation of nanoscopic particles. Thus, the initial precursor for the formation of the final product was obviously a new mixed acetate. Indeed, by evaporating the methanol and all volatiles, we obtained a solid which showed a new XRD powder pattern (Fig S2, ESI†). No reflections of the former pure acetates were detected. The new compound can be re-crystallized from water keeping unchanged its XRD powder pattern. We were able to grow single crystals of the new compound, $[(H_2O)Yb(CF_3COO)_2(CH_3COO)]_n \cdot n[CH_3COOH]$ from water solutions and solved its solid state structure by X-ray single crystal analysis. It crystallizes in the triclinic space group P $\bar{1}$ with Z = 2. The X-ray structure of the new compound shows the composition of an ytterbium complex with acetato and trifluoroacetato ligands directly bound to Yb^{III}, as expected. The crystallographic data reveal that Yb^{III} atoms in the new complex $[(H_2O)Yb(CF_3COO)_2(CH_3COO)]_n \cdot n[CH_3COOH]$ (**1**) are connected

through different acetato- and trifluoroacetato- bridging modes forming the catena structure of **1.** The asymmetric unit contains one Yb^{III} atom coordinated by eight oxygen atoms ($\sigma^8\lambda^3$-Yb) of three different ligands (acetato, trifluoroacetato and aqua) as well as one uncoordinated acetic acid molecule (Figure 1i). Whereas the water is bound on Yb^{III} "pure terminally" (O9), all coordinated acetates act as bridging ligands. Three symmetry-related Yb^{III} atoms build up the basic two subunits of the structure, each comprised of two metal centers: two Yb^{III} atoms are linked through four μ2-trifluoroacetato-briges (O3, O4, O5, O6) forming a centrosymmetric binuclear unit with Yb…Yb distances of 4.4641(12) Å., nearly the same as in the well-known tris(trifluoroacetato) trihydrates of RE metals.[17,18] The acetato ligand affects twofold the structural motif of **1**: Firstly, it acts with both oxygen atoms (O7, O8) as a bidentant ligand on each Yb^{III} atom and secondly, it connects the former triflouroacetato-ytterbium-binuclear subunits to a polymeric chain *via* a μ-oxygen (O7), completing the 8-fold symmetry at each Yb^{III} center by forming a new Yb-O-Yb-O-ring with Yb…Yb distances of 3.9518(11) Å. Similar four-member structural fragment was also determined in the crystal structure of ytterbium triacetate tetrahydrate.[19] Figure 1ii shows the extended fragment constructed from both binuclear entities as the main feature of the catena structure of **1**. Note that due to the inversion center, the aqua ligands (O9) alternate their orientations (*trans* to each other) at the Yb^{III} atoms of the polymeric chain.

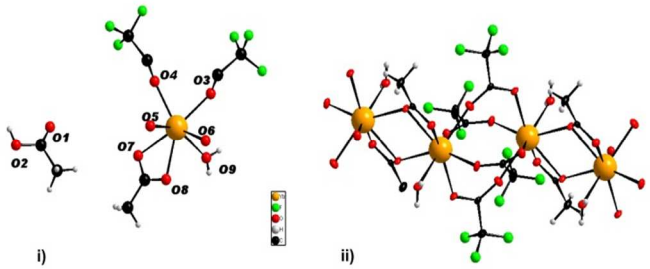

Fig 1: i) Asymmetric unit representing complex **1** ii) cut-out of the polymeric chain (CH_3COOH- solvate molecules are omitted for clarity)

After adding two equivalents of HF to the ytterbium precursor solution, a transparent sol of high concentration was formed. The resulted sol is stable for a few months and can be handled and stored at air. Just to mention, by adding 3 equivalents of HF, precipitation of agglomerates was observed. So, similar to the fluorolytic sol-gel synthesis of aluminium fluorides,[20] operating substoichiometrically is recommended in order to obtain transparent sols. Thus, the final product can be described as $YbF_{3-x}(O_2CCF_3)_x$ with x~1. The reaction pathway can be expressed as follows:

$$Yb(O_2CCH_3)_3 \xrightarrow[-\ CH_3COOH]{2\ CF_3COOH,\ MeOH} \underset{\mathbf{1}}{[(H_2O)Yb(O_2CCF_3)_2(O_2CCH_3)]_n \cdot n\ [CH_3COOH]} \xrightarrow[-\ CH_3COOH\ -\ CF_3COOH]{(3-x)\ HF_{MeOH}} YbF_{3-x}(O_2CCF_3)_x$$

DLS was used to monitor the average hydrodynamic diameter of sol particles and to study the change in particles size with increasing concentration and increasing aging time of the sols. Figure 2i shows the size distribution by intensity of sols with concentrations of 0.1 M, 0.5 M and 1 M. All three sols show a size distribution with two maxima. The 0.1 M sol having the lowest dynamic viscosity of 0.619 mPas has the largest particles with a hydrodynamic diameter of approx. 10 and 220 nm. The sol of the highest concentration (1 M) is having the highest viscosity (1.236 mPas) with the particle size to be the smallest with approx. 3 and 70 nm. Since the size distribution by intensity is supposed to overestimate larger particles or agglomerates by a factor 10^6, figure 2ii presents the size distribution by volume with only one maximum. With increasing concentration the maxima shift to smaller values indicating the presence of particles with smaller hydrodynamic diameters. This tendency can be rationalized by the fact that nuclei formation proceeds faster than nuclei growth. Hence, the following particle growth is controlled by the restricted availability of molecular precursors that are faster consumed thus terminating any further mass transport. Maintaining a constant sol volume, the increase in viscosity can be attributed to different physical effects, which result from the relationship between particle size and concentration. Since DLS clearly indicates smaller particle formation due to the kinetic effect described above, the concentration of solid particles per volume fraction significantly rises up. This causes a strengthening of particle-particle interactions resulting in an increase in viscosity. Consequently, a larger amount of smaller particles influences the dynamic viscosity of sols. The 1 M sol does not only have a concentration of 10 times higher than the 0.1 M sol but it also exhibits particles with hydrodynamic diameters 3 times smaller. The volume fraction of the 1 M sol consists of a large amount of very small solid particles wherefore the resistance in movement and flow increases and viscosity rises significantly. The 0.5 M sol lies between the two above in terms of concentration, particle size and viscosity (0.804 mPas). Thus, these results show a concentration dependence of the hydrodynamic particle size in ytterbium fluoride sols.

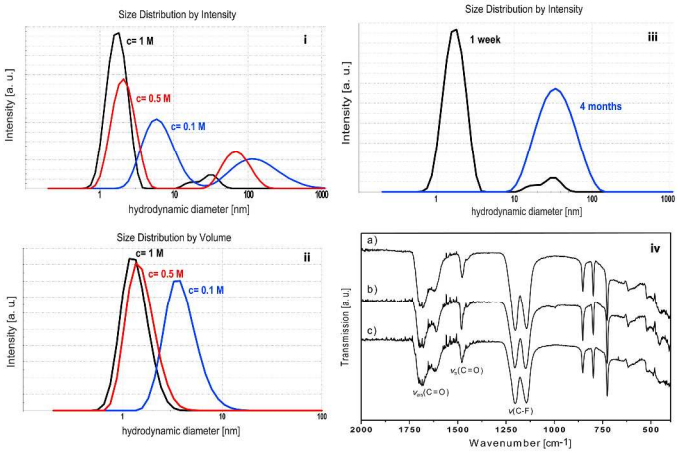

Fig 2: Size distribution by intensity (i) and volume (ii) of sols of different concentrations. iii) DLS size distribution by intensity of a 1 M sol at different aging times. iv) IR spectra of $YbF_{3-x}(O_2CCF_3)_x$ xerogel obtained from a transparent 0.1 M sol (a) from a turbid 1 M sol (b) and from a precipitate after its sedimentation (c).

The determination of crystallite sizes according the Scherrer equation would possibly support the results but the xerogels obtained from transparent sols are X-ray amorphous. The results from XRD measurements are presented in figure 3. The X-ray powder diffraction pattern of the $YbF_{3-x}(O_2CCF_3)_x$ xerogel shows no reflections indicating that the xerogel obtained from the sol is X-ray amorphous. After calcining the xerogel at higher temperatures *e.g.* 300 °C and 500 °C narrow reflections of the orthorhombic YbF_3 become visible, thus indicating the decomposition of the unreacted trifluoroacetate group at higher temperatures and formation of the stable YbF_3.

Additionally, to gain further information on particle size, morphology and crystallinity of nanoparticles, TEM investigations were performed. Apparently, the sol coating shows no particles by material contrast leading to the conclusion that an amorphous

material is obtained and no particle size can be evaluated from the TEM image (Fig S1, ESI†). The results are well in agreement with the XRD measurement (see Fig.3).

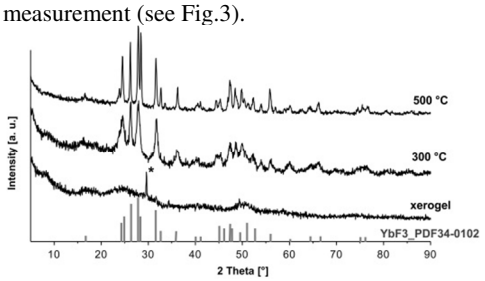

Fig 3: X-ray diffraction of the obtained xerogel at different calcination temperatures, reflection from the sample holder is marked with *.

Depending on the concentration the obtained sols age at different rates. While the low concentrated sol shows neither loss of transparency nor sol-gel transition over a period of 2 years, the sol with high concentration becomes turbid within months indicating the formation of larger agglomerates. This is demonstrated by DLS measurements (Fig. 2iii). The size distribution by intensity of a 1 week aged sol shows 2 maxima at 3 and 70 nm. The 4 months aged sol shows only one maximum at 70 nm. Immediately after fluorination 2 classes of particle size are present in the sol. Since the larger particles are overestimated, the particles of the smaller size of *approx*. 3 nm are in the majority. In the course of a few months the transparent sol becomes gradually more turbid. It can be assumed that during that time the small particles agglomerate to form larger units in order to lower the surface energy and to reach a thermodynamically stable state. After 4 months only larger agglomerates are present as only one maximum in the particle size distribution can be detected. As the aging proceeds, the sol becomes more turbid until a certain degree of turbidity is reached and a subsequent precipitation is observed after *approx.* 6 months. Meanwhile the 0.1 M does not show any signs of sol aging. Due to the difference in concentration the number of solid particles is lower. Also, DLS measurements show that the sol particles are larger than in the 1 M sol (see Fig 2i). Hence, less particle-particle interactions occur, compared to sols of higher concentration, and therefore the agglomeration proceeds slower. Since ytterbium (III) compounds are paramagnetic, application of NMR techniques is inappropriate. In addition, XRD experiments are also not suitable for investigating structural changes as the xerogels are X-ray amorphous. For that reason IR spectroscopy was used to gain information on possible structural changes with increasing aging time. Figure 2iv shows the IR spectra of an $YbF_{3-x}(O_2CCF_3)_x$ xerogel obtained from a transparent 0.1 M sol, a xerogel obtained from a turbid 1 M sol and a precipitate after its sedimentation. The IR spectra exhibit the expected vibrations derived from unreacted TFA-groups in the samples. This is demonstrated by the (asymmetrical and symmetrical) stretching vibration of carbonyl groups at 1690-1612 cm^{-1} and at 1477 cm^{-1} and by the vibration of the C-F group at 1142-1202 cm^{-1}. As no significant change is shown in the IR spectra, one can conclude that the turbidity and increase in particle size is a result of the proceeding agglomeration process which is caused by physical parameters mentioned above rather than by a change in the chemical structure of the particles.

Conclusion

In this study, the preparation of highly transparent ytterbium fluoride sols of high concentration and low viscosity by the fluorolytic sol-gel synthesis is presented for the first time. The particle size determined by DLS can be found in the lower nm range. Additionally, DLS studies show a concentration dependency on particle size. Furthermore, DLS and IR spectroscopy were used to study the aging behavior of the sols. With increasing aging time, the sols become more turbid until sedimentation is observed. This process is based on the particles' tendency to agglomerate in order to reduce their surface energy and also depends on the concentration of the sols. The xerogel consists of agglomerated nanoparticles that remain amorphous at room temperature. XRD studies confirm the formation of YbF_3 at higher temperatures. The new Yb^{III} compound has been characterized giving structural information of the initial precursor. The main advantage of this precursor is its solubility and easy exclusion of water during the reaction. The presented fluorolytic sol-gel synthesis offers an easy and efficient access to nanoscopic ytterbium fluorides which, due to their nanoscopic size and amorphous character, can exhibit a high catalytic activity in selected reactions. Moreover, the sols are characterized by a high transparency, low viscosity and long term stability and therefore are suitable for further processing in the fields of medicine, dentistry and optics. Especially the preparation of inorganic-organic nanocomposites is of great interest in material science. This work is currently ongoing in our group.

The authors would like to thank Beatrice Braun for support with the single crystal structure refinement and Holm Kirmse (Humboldt-Universität zu Berlin, Department of Physics) for TEM measurements. L. Schmidt is a member of the graduate school GRK 1582 "Fluorine as a Key Element" of DFG (Deutsche Forschungsgemeinschaft).

Notes and references

[a] Humboldt-Universität zu Berlin, Department of Chemistry, Brook-Taylor-Straße 2, 12489 Berlin, Germany, erhard.kemnitz@chemie.hu-berlin.de

† Electronic Supplementary Information (ESI) available: detailed experimental procedures, TEM image, XRD powder pattern and X-ray crystal structure solution of **1** (CIF). See DOI: 10.1039/c000000x/

1. A. Wiegand, W. Buchalla, and T. Attin, *Dent. Mater.*, 2007, **23**, 343–62.
2. K. Rosin-Grget and I. Lincir, *Coll. Antropol.*, 2001, **25**, 703–12.
3. G. Furtos, V. Cosma, C. Prejmerean, M. Moldovan, M. Brie, A. Colceriu, L. Vezsenyi, L. Silaghi-Dumitrescu, and C. Sirbu, *Mater. Sci. Eng. C*, 2005, **25**, 231–236.
4. H. H. K. Xu, J. L. Moreau, L. Sun, and L. C. Chow, *Biomaterials*, 2008, **29**, 4261–7.
5. T. C. S. Oliveira, E. Piva, F. B. Leal, M. D. Moncks, and C. W. Raubach, *Nano-Micro Lett.*, 2012, **4**, 189–196.
6. I. Mohamed Hamouda, *J. Biomed. Res.*, 2012, **26**, 143–51.
7. H. H. K. Xu, J. L. Moreau, L. Sun, and L. C. Chow, *J. Dent. Res.*, 2010, **89**, 739–45.
8. X. Wang, J. Zhuang, Q. Peng, and Y. Li, *Inorg. Chem.*, 2006, **45**, 6661–5.
9. Y.-P. Du, Y.-W. Zhang, L.-D. Sun, and C.-H. Yan, *Dalton Trans.*, 2009, 8574–81.
10. P. P. Fedorov, A. a. Luginina, S. V. Kuznetsov, and V. V. Osiko, *J. Fluor. Chem.*, 2011, **132**, 1012–1039.
11. V. Bartůněk, J. Rak, Z. Sofer, and V. Král, *J. Fluor. Chem.*, 2013, **149**, 13–17.
12. M. Siemons, T. Weirich, J. Mayer, and U. Simon, *Zeitschrift für Anorg. und Allg. Chemie*, 2004, **630**, 2083–2089.
13. M. He, P. Huang, C. Zhang, F. Chen, C. Wang, J. Ma, R. He, and D. Cui, *Chem. Commun. (Camb).*, 2011, **47**, 9510–2.
14. L. Pan, M. He, J. Ma, W. Tang, G. Gao, R. He, H. Su, and D. Cui, *Theranostics*, 2013, **3**, 210–22.
15. E. Kemnitz, U. Gross, S. Rüdiger, and C. S. Shekar, *Angew. Chem. Int. Ed. Engl.*, 2003, **42**, 4251–4.
16. S. Rüdiger and E. Kemnitz, *Dalton Trans.*, 2008, 1117–27.

17. V. I. Belyi, A. A. Rastorguev, A. A. Remova, G. V Romanenko, and N. P. Sokolova, *J. Struct. Chem.*, 2002, **43**, 587–594.
18. C. J. Kepert, L. Wei-Min, P. C. Junk, B. W. Skelton, and A. H. White, *Aust. J. Chem.*, 1999, **52**, 459–480.
19. R. Vadura and J. Kvapil, *Mater. Res. Bull.*, 1971, **6**, 865–873.
20. C. Fritz, G. Scholz, M. Feist, and E. Kemnitz, *Dalton Trans.*, 2012, **41**, 11351–60.

